Journal of Applied Physics ARTICLE pubs.aip.org/aip/jap

Direct density modulation of photo-assisted field emission from an RF cold cathode

Cite as: J. Appl. Phys. 134, 074904 (2023); doi: 10.1063/5.0156328
Submitted: 28 April 2023 · Accepted: 30 July 2023 ·
Published Online: 16 August 2023

Lan Jin, Yang Zhou, and Peng Zhang[a)]

AFFILIATIONS

Department of Electrical and Computer Engineering, Michigan State University, East Lansing, Michigan 48824-1226, USA

[a)]**Author to whom correspondence should be addressed:** pz@egr.msu.edu

ABSTRACT

This paper explores direct density modulation of high-current electron beam emission from an RF cold cathode using optical excitation. We theoretically study the photo-assisted field emission of periodically bunched electron beams of various pulse shapes under the combined excitation of an RF field and an optical field, using an exact quantum model. Both continuous-wave (CW) and pulsed optical fields are considered. The emission current pulse amplitude, pulse width, electron number density per pulse, as well as pulse shape and its harmonic contents are investigated in detail. For CW photon sources in the UV to NIR range (i.e., 200–1200 nm), increasing the optical intensity under an RF bias tends to change the current pulse from a Gaussian to sinusoidal-like shape, thus offering strong flexibility to control the frequency components in beam current emission. Pulsed photon sources combined with an RF field can produce sharp, high-current electron bunches with pulse duration comparable with or even less than that of the optical pulse. A contour map of the density modulation depth is constructed for different combinations of RF and laser fields. The results provide insight into unlocking new opportunities to achieve direct density modulation during electron current emission by optical means.

I. INTRODUCTION

Electron beam-based devices are critical to applications such as particle accelerators,[1] high-power electromagnetic sources ranging from microwaves to x-rays,[2–5] vacuum electronic devices,[6–9] e-beam lithography,[5] electron microscopy,[10–13] space-vehicle neutralization,[14] and emerging vacuum nanodevices.[15–18] They are key elements in telecommunication systems, satellite-based transmitters, radar, communication data links, and electronic countermeasures.[19] There continues to be strong interest in increasing the output power, frequency tunability, and bandwidth of electron beam-based vacuum electronics devices, for uses as radiation sources and power amplifiers, from GHz to THz and beyond.[20–23]

Free-electron beam-based devices utilize the collective interaction of an electron beam with a circuit structure (e.g., either periodic structure or cavity) to convert electron beam energy into electromagnetic radiation. The energy conversion from electron beams into electromagnetic radiation relies on beam modulation.[21,24] Beam modulation is achieved either by controlling the electron emission from the cathode (prebunching) or by passing the electrons through an RF electric field structure that modulates the velocities of the electrons. The former is referred as density modulation, whereas the latter is as velocity modulation in the literature.[21,25] One may keep in mind that, strictly speaking, density modulation and velocity modulation of the beam cannot be separated as can be seen from the (linearized) continuity equation; thus, they were used only to distinguish the different ways of initiation of the beam modulation. At present, traveling wave tubes (TWTs) mainly rely on the velocity modulation of the electron beam for power amplification. After the electron velocities are modulated, there is a substantial delay before beam density modulation becomes appreciable, until when the useful gain is produced. Dramatic improvements in TWT performance can be enabled by direct density modulation (i.e., prebunching of electron beam) during emission.[26] In particular, with this initial density modulation, velocity dispersion in the beam can be minimized, and the substantial portion of the interaction circuit for the purpose of converting initial velocity modulation into sufficient density modulation can be eliminated. This would result in compact devices with reductions in overall dimensions and weight, through the elimination of the premodulation circuit. Furthermore, initial beam density modulation during emission would eliminate the launching loss of the input RF signal, which is a serious intrinsic problem in TWTs based on initial velocity modulation.[27,28]

The idea of using direct current modulation of electron beams in microwave amplifiers has existed for decades. Density modulation in amplifiers has gone by the name of inductive output amplifiers (IOAs).[25] Historically, density modulation was accomplished with a grid that lays over the surface of a thermionic emitter to control the electron emission.[25,29–31] With the advancement of vacuum microelectronics and field emitter arrays (FEAs), the gate-to-emitter spacing has been reduced to submicron scale, which significantly decreases the electron transit time, thus offering a higher frequency operation.[32] However, the capacitance of the field emitter arrays always limits the modulation frequency. Also, there are significant challenges for using FEAs in high-power tubes, because premature failure due to arcing often occurs at current levels much smaller than the design requirements.[33] The breakdown is a major challenge for FEAs because of the high fields within the structure and the thin-film gate electrode. An electrical short between the gate and any individual emitter will burn out the entire FEA and render it unusable.[34] While shields can be added to mitigate the damaging effects of the electrical shorts, the high operating voltage is needed to field emitter arrays to draw sufficient current.

In this paper, we explore direct density modulation of high-current electron beam during its emission from an RF cold cathode using optical excitation. This is motivated by the recent rapid development in ultrafast lasers and photonics, which has opened up enormous opportunities to control electron beam dynamics at ultrashort spatial-temporal scales, thus offering unprecedented scientific advances. Pulsed laser-induced (or assisted) electron emission offers the possibility of manipulation and control of coherent electron motion in ultrashort spatiotemporal scales.[1,33,35] The timing of electron beam emission, and therefore of the electron beam density modulation, can be achieved in femtosecond scale (well beyond the RC limit of the emitters), by laser illuminating DC-biased sharp metallic tips.[36,37] This ultrafast electron emission due to pulsed laser, or optical gating, would potentially provide unrivaled precision in phase-control of electromagnetic signals from electron-based devices.

There have been efforts to use laser illumination of photocathodes to achieve microwave amplification with high efficiency; however, the development of such devices, i.e., the so-called lasertron,[38,39] was inhibited largely because of the lack of reliable and affordable electron emitters in the 1980s. With recent advances in materials and nanotechnology, there appear a variety of robust electron emitters with promises for high-current applications, e.g., carbon fibers,[40–42] carbon nanotubes (CNTs), and carbon nanofiber (CNF)[43–48] based field emitters. Also, cathode geometry has been investigated to enhance emission.[49] Excitation of field emitters with photon sources would offer potential to control the emission current with strong flexibility.

It has been shown that photo-assisted field emission current under the combination of static bias and optical field is significantly larger than either photoemission due to the optical field alone or field emission due to static field alone.[50–53] Because of the high nonlinearity of photo- and field-emission, the combined RF bias and optical fields are expected to produce agile current pulse shapes tailored for specific applications. Another advantage of optical gating is that, in the case of emitter arrays, individual emitters can be selectively excited using prescribed optical gating. This selective gating would be able to produce multiple electron beams with separate modulations simultaneously, by various combinations of field emission, photoemission, and even thermionic emission. The proposed photo-assisted field emission requires greatly reduced RF (or DC) bias to achieve high current compared to the traditional FEAs, which can help prevent instability induced by poor vacuum conditions when pressed local biased electric field at the emitter tip is close to the field emission threshold. Furthermore, the occurrence of arcs is diminished as the relevant heating effect due to photoelectron emission is restrained when the pulses are in a short temporal duration.[54] Thus, the issue of breakdown can be mitigated to provide a more stable and robust emitter operation.[55]

Here, we theoretically analyze the emission of periodically bunched electron beams under the excitation of an RF field and an optical field, using an exact quantum model.[50,56,57] We apply a sinusoidal RF electric field (1 GHz) and an optical field (wavelength from 200 to 1200 nm) simultaneously to a cold cathode. Electron emission properties, such as peak current density, current pulse width, pulse shape, its corresponding harmonic contents, and electron numbers per RF cycle, are comprehensively analyzed for a wide range of RF field and optical field [i.e., wavelength, laser intensity, and continuous-wave (CW) or pulsed form]. Note that we consider a representative RF frequency of 1 GHz for this study, however, frequencies of 10 GHz or higher may be even more interesting with our proposed optical method, where thermionic cathodes are precluded from competing and standard field emission cathodes are challenged.

II. QUANTUM MODEL FOR ELECTRON EMISSION

As shown in Fig. 1, we consider electron emission from an RF cold cathode under an RF field F_0 and an optical field $F_1\cos\omega t$, where F_1 and ω are the optical field strength and its angular frequency, respectively. The RF field is $F_0 = A\cos\omega_0 t$, with A and ω_0 being the amplitude and angular frequency of the RF field, respectively. For RF fields of GHz frequency, it has a period (~ns) that is orders of magnitude longer than that of the optical field, e.g., 0.67–4 fs for wavelengths in the range of 200–1200 nm (UV–NIR). Therefore, the RF field can be regarded as a constant static field in one or multiple laser cycles. Consequently, the photo-assisted field emission induced by the combination of RF and optical fields is modeled using our recently developed quantum model by solving the one-dimensional (1D) time-dependent Schrödinger equation (TDSE) exactly,[50,56,57] which is applicable for the arbitrary static electric field, emitter properties (i.e., Fermi energy, work function, and with or without dielectric coatings[58,59]), and optical field (i.e., wavelength and strength). The quantum model has shown good agreement with experiments[56,57] and it has been extended to various scenarios, such as two-color laser-induced photoemission,[51,53,60,61] few-cycle pulsed laser-induced photoemission,[52] electron emission from dielectric-coated metal surfaces,[58,59,62] and electron emission in the nanogaps.[63,64]

To model the time-dependent oscillating surface barrier [Fig. 1(b)], for simplicity, both the RF field and optical field are assumed to be perpendicular to the cathode surface and cut off at the cathode–vacuum interface. The Schottky barrier lowering $2\sqrt{e^3F_0/16\pi\varepsilon_0}$ due to the image charge effect is included, where e is the (positive) elementary charge and ε_0 is the permittivity in free space. It should be noted that our analytical model uses a triangular barrier only, where barrier correction factors[65] and the effect of possible changing barrier height due to an oscillating optical field are

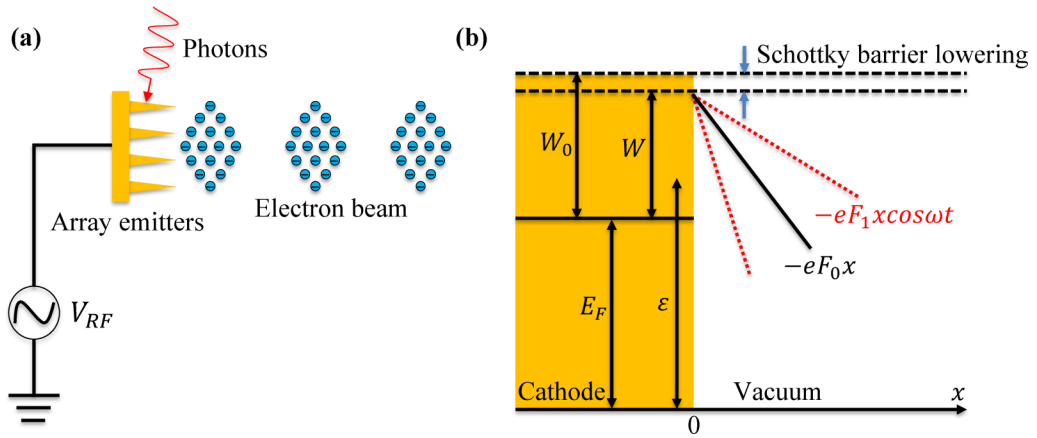

FIG. 1. (a) The periodical emitted bunched beam produced from sharp emitter array under an RF field and a laser field. (b) The quantum model with a one-dimensional solid-vacuum interface under an RF field F_0 and a laser field $F_1\cos\omega t$, with E_F being the Fermi energy, W_0 the work function of the cathode, ε the initial energy, and W the effective work function considering the Schottky effect.

not considered, which may be subjects of future studies. Based on the exact solution of TDSE subject to the oscillatory surface barrier due to the RF static and laser fields,[50,56] we obtain the time-averaged electron transmission probability from the energy level of ε,

$$D(\varepsilon) = \sum_{n=-\infty}^{\infty} w_n(\varepsilon), \tag{1}$$

where $w_n(\varepsilon)$ denotes the electron transmission probability through the n-photon process, with $n<0$ representing multiphoton emission process, $n=0$ direct tunneling process, and $n>0$ multiphoton absorption process. The detailed expressions $w_n(\varepsilon)$ can be found in Refs. 50 and 56.

Thus, the total emission current density J in a laser cycle can be calculated by

$$J = e\int_0^{\infty} D(\varepsilon)N(\varepsilon)d\varepsilon, \tag{2}$$

where $N(\varepsilon) = \frac{mk_BT}{2\pi^2\hbar^3}\ln\left[1+\exp\left(\frac{E_F-\varepsilon}{k_BT}\right)\right]$ is the supply function derived from the free-electron model for metal, with E_F, k_B, and T being the Fermi level, the Boltzmann constant, and the temperature, respectively, and $N(\varepsilon)d\varepsilon$ gives the flux of electrons inside the metal impinging normal on the metal surface with initial energy between ε and $\varepsilon+d\varepsilon$.[56]

To explore the flexibility of density-modulated electron beam emission, we consider the combination of RF fields with either CW or pulsed photon/laser sources, as illustrated in Fig. 2. The latter is motivated by the fs scale of the timing of the photoelectron emission under pulsed laser illumination. High-frequency beam modulation with precise bunch profiles may be easily realized by the optically gated emitters. It is desirable to produce a train of tightly bunched electrons at a repetition rate of the microwave frequency, in order to achieve synchronism between the electron bunch and the microwave for effective interaction. One possible approach is to use the RF signal $A\cos\omega_0 t$ to trigger the laser at a certain

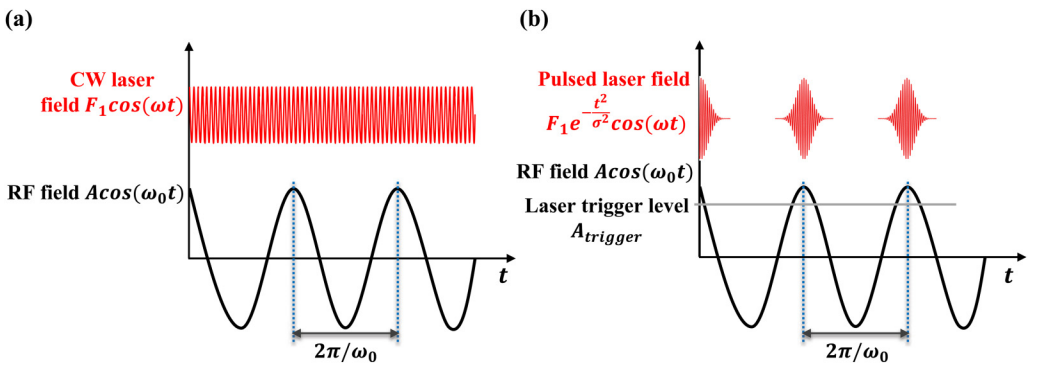

FIG. 2. Cathode excitation using (a) an RF field and a CW laser field, (b) an RF field and a pulsed laser field. The laser pulse is triggered by an RF field at a certain voltage level.

predetermined level $A_{trigger}$, so that high-current electron emission occurs only when the laser is triggered [Fig. 2(b) and Fig. 8]. The electron bunch length can be controlled by tuning the trigger level voltage $A_{trigger}$. Because of the finite rise and fall time of the laser pulse, instead of a constant amplitude of F_1 as for the CW laser, the amplitude of the pulse laser is modeled as $F_1 e^{-t^2/\sigma^2}$, where F_1 is the peak of the optical field, and $\sigma = \frac{\tau_p}{2\sqrt{\ln 2}} \cong \frac{\tau_p}{1.665}$, with τ_p being the full width at half maximum (FWHM) of the optical pulse length. We assume that the laser pulse length is much longer than the laser period (i.e., more than 10 laser cycles[50,52]) so that the laser amplitude $F_1 e^{-t^2/\sigma^2}$ can be seen as a constant within a laser cycle and Eqs. (1) and (2) can still be applied to calculate the emission current density.

It is important to note that the field magnitudes A and F_1 used here are the local field strength at the cathode surface, which may be significantly larger than the input RF and/or optical fields if one considers the large local field enhancement near the sharp emitter tips. The external input fields needed to yield the presented current density level would be lowered according to their corresponding field enhancement factors, i.e., $F_{input-RF} = A/\beta_{static}$ and $F_{input-optical} = F_1/\beta_{optical}$, where the local field enhancement factors for RF field β_{static} and optical field $\beta_{optical}$ are typically on the order of 10^4–10^5 and 10, respectively.[45–47,59] As the frequency of the field increases from DC/RF to optical range, the skin depth increases and can become comparable to or even larger than the physical size of the tip, thus, the electric field can penetrate inside the material and the screening effect of free electrons inside the emitter becomes less effective, yielding a significantly reduced field enhancement factor for optical field as compared to the DC/RF field. Techniques such as surface coating, designing tip geometry with plasmonic resonance enhancement, and resonant tunneling[59,62,66,67] can further increase the local field enhancement and reduce the input RF and optical field strengths in practice.

III. RESULTS AND DISCUSSION

A. Electron emission under RF field and continuous laser field

Figure 3 shows the periodic bunched emission current density J calculated from Eq. (2) during the positive RF half-cycles under various combinations of laser and RF field strength. The cathode is assumed to be gold, with nominal work function $W_0 = 5.1$ eV and Fermi energy $E_F = 5.53$ eV. The temperature is $T = 300$ K. Unless prescribed otherwise, these are default cathode properties in this study. The laser has a wavelength of 200 nm, and its heating effects are ignored due to the weak laser intensity used.[57,68] RF field has a frequency of 1 GHz, with its negative half-cycles being neglected in the calculation.

The RF field magnitudes A corresponding to curves in green, blue, red, yellow, and purple [bottom to top in each subfigure in Figs. 3(b)–3(d)] are 0, 0.1, 1, 2, and 3 V/nm, respectively. In Fig. 3(a), we plot emission current density J under the RF field only with $A = 1$, 2, and 3 V/nm (bottom to top) calculated from Eq. (2), which are almost identical to the current density calculated (black dotted line) from the Fowler–Nordheim (FN) approximation

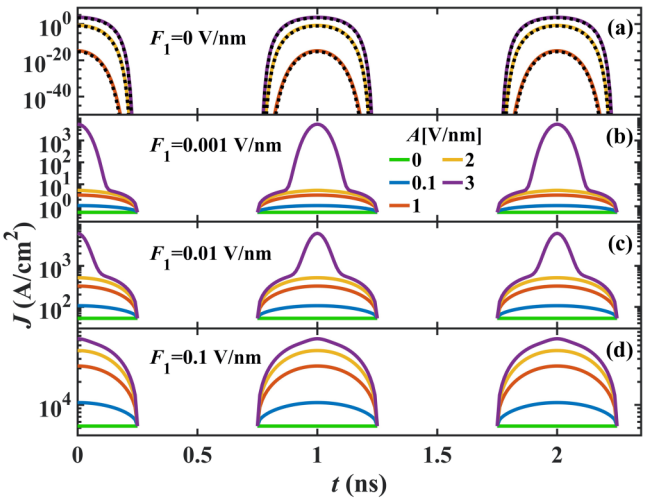

FIG. 3. Electron emission current density J varies with t under different combinations of RF field strength and laser field strength. The amplitude of the RF field A corresponding to curves in green, blue, red, yellow, and purple (bottom to top in each subfigure) is 0, 0.1, 1, 2, and 3 V/nm, respectively. The frequency of the RF field is 1 GHz. In (a), current density under RF only ($F_1 = 0$) is plotted, and the dotted black lines are plotted from the FN approximation, Eq. (3). The laser field has a wavelength of 200 nm and strength F_1 = (b) 0.001, (c) 0.01, and (d) 0.1 V/nm.

equation,[65,69]

$$J = \alpha a W^{-1} F_0^2 \exp\left(-\frac{\beta b W^{\frac{3}{2}}}{F_0}\right), \tag{3}$$

where $a \approx 2.46\ 965 \times 10^{-25}$ A J V^{-2} and $b \approx 1.06\ 5\ 15 \times 10^{38}$ J$^{-3/2}$ V m^{-1} are the first and second FN constants, and $\alpha = 1$ and $\beta = 1$ are generalized correction factors. The emission current density for the cases under only laser fields of 0.001, 0.01, and 0.1 V/nm reads 0.5, 53, and 5282 A/cm^2, respectively, as shown at the bottom of Figs. 3(b)–3(d), which are much larger than that of with RF field only in Fig. 3(a). With the 10 times increase of laser field, the corresponding emission current density is increased by about 100 times without the RF field. As the laser field increases from 0.001 to 0.1 V/nm with the RF field, as shown in Figs. 3(b)–3(d), the peak emission current density increases from 1 to 10 715 A/cm^2 for $A = 0.1$ V/nm. A larger A increases the emission current density even further. Thus, the presence of photons provides significant flexibility in controlling the emission current. More importantly, the shape of the temporal emission current density J varies in different combinations of the RF amplitude and laser field. From Figs. 3(a)–3(d), we observe when the RF field dominates the emission process (i.e., large RF field but small laser field), the shape of the temporal emission current density is in a Gaussian profile. When increasing the laser field, the current density profiles change toward a sinusoidal shape.

Figures 4(a)–4(c) show the emission current density J in positive RF half-cycles with RF field amplitude $A = 2$, 2.5, 3 V/nm,

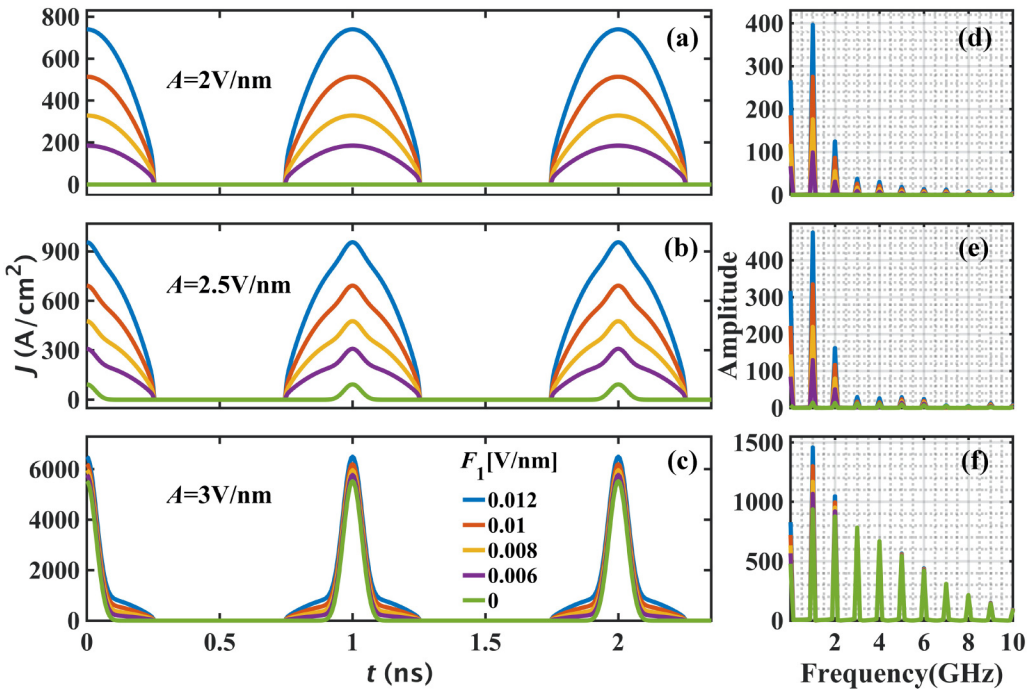

FIG. 4. (a)–(c) Emission current density J varies with time t in 2.5 cycles under various laser fields with the RF amplitude A = 2, 2.5, and 3 V/nm, respectively. (d)–(f) The amplitude spectrum of the emission current density at the multiples of RF frequency (1 GHz) for (a)–(c) correspondingly. The laser wavelength is 200 nm.

respectively. The lines varying in color green, purple, yellow, red, and blue (bottom to top in each subfigure) correspond to $F_1 = 0$, 0.006, 0.008, 0.01, 0.012 V/nm. The corresponding optical intensities $I[\mathrm{MW/cm^2}] = \varepsilon_0 c F_1^2/2 = 1.327 \times 10^5 \times (F_1[\mathrm{V/nm}])^2$ are 0, 4.8, 8.5, 13.3, 19.1 MW/cm^2, where c is the speed of light in vacuum, for linearly polarized lasers. When $A = 2$ V/nm, those curves can be fitted with a sinusoidal function of a magnitude of 740, 514, 329, 185, 0.18 A/cm^2 from top to bottom and a frequency of 1 GHz. As A increases, the shape of the emission current changes from an approximately sinusoidal shape to a Gaussian-like profile, similar to Fig. 3. Because of the high nonlinearity of photo-assisted field emission, increasing A produces a sharp peak in the middle, and the width of the peak becomes narrower, as shown in Figs. 4(b) and 4(c). It is also found that as A increases from 2 to 3 V/nm, the difference in emission current under different laser fields gets smaller. This is because the RF field is much larger than the laser field, and it plays the dominant role in modulating the emission current.

A frequency domain analysis of the emission current is done using the fast Fourier transform (FFT). The amplitude spectrum of emission current density at multiples of RF frequency (1 GHz) is shown in Figs. 4(d)–4(f) for Figs. 4(a)–4(c), respectively. The dominant frequency term is observed at 1 GHz, which is the same as the frequency of the RF field. As A increases, there appear more high-harmonic contents in the beam current, as shown in Fig. 4(f). For a given A, increasing the laser field tends to increase more on the fundamental frequency component in the emission current.

The effect of the RF field on the modulation of electron beams is provided in Fig. 5, with different laser fields of 0, 0.006, 0.008, 0.01, 0.012 V/nm, corresponding to the intensity of $I = 0$, 4.8, 8.5, 13.3, 19.1 MW/cm^2. Figure 5(a) shows that the peak emission current density increases with the RF field. When $A = 3$ V/nm, the peak emission current density remains almost unchanged for the given range of laser intensity due to the dominant direct tunneling under the RF field. Figure 5(b) shows the FWHM of the emission current density under different RF fields. When $A = 2$ V/nm, there is a sharp increase of FWHM as I increases from 0 to 4.8 MW/cm^2. FWHM remains constant as I further increases. When $A = 2.5$ V/nm, after the sharp increase of FWHM as I increases from 0 to 4.8 MW/cm^2, FWHM gradually increases as I further increases. When $A = 3$ V/nm, FWHM almost keeps constant since RF field strength is much larger than the laser field and the modulation by the laser field becomes weak. Figure 5(c) shows the number of emitted electron flux per RF cycle, N, which is calculated by,

$$N = \frac{1}{e}\int_0^{2\pi/\omega_0} J(t)dt, \tag{4}$$

where $J(t)$ is the temporal emission current density calculated from Eq. (2). It is interesting to find that N has similar trends as peak emission current density. This may indicate that for CW lasers, the laser intensity has a stronger influence on the emission current amplitude and a weaker influence on the modulation of beam width,

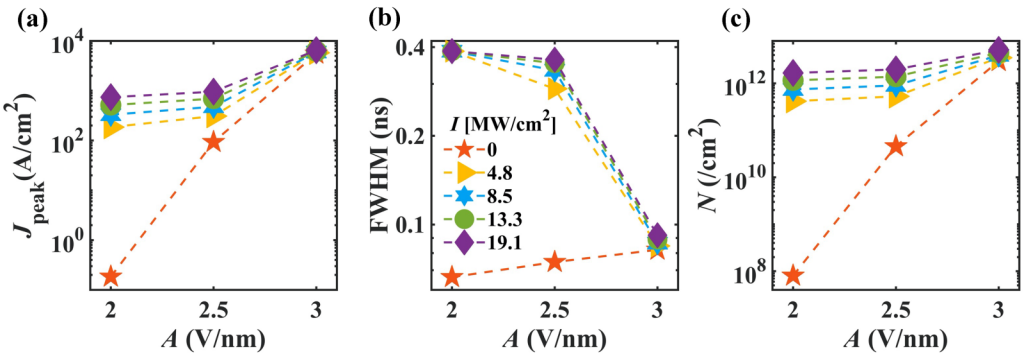

FIG. 5. (a) Peak emission current, (b) full-width at half maximum (FWHM), and (c) number of emitted electrons in a half RF cycle, as a function of RF field A under different laser intensity I. The laser wavelength is 200 nm.

especially when the RF field is much larger than the laser field strength.

The effect of laser wavelength on the emission current density is shown in Fig. 6. For fixed laser and RF field strength, emission current density decreases rapidly as laser wavelength increases. This is because of the lower quantum efficiency for longer laser wavelengths.[57] When F_1 increases from 0.006 to 0.012 V/nm, the peak emission current density increases from 185 to 740 A/cm^2 for $\lambda = 200$ nm and from 0.20 to 0.23 A/cm^2 for $\lambda = 1000$ nm. A shorter wavelength laser has stronger effects on the modulation of the emission current. It is also observed that as the laser wavelength increases, the peak width decreases. Figures 6(e)–6(h) show the

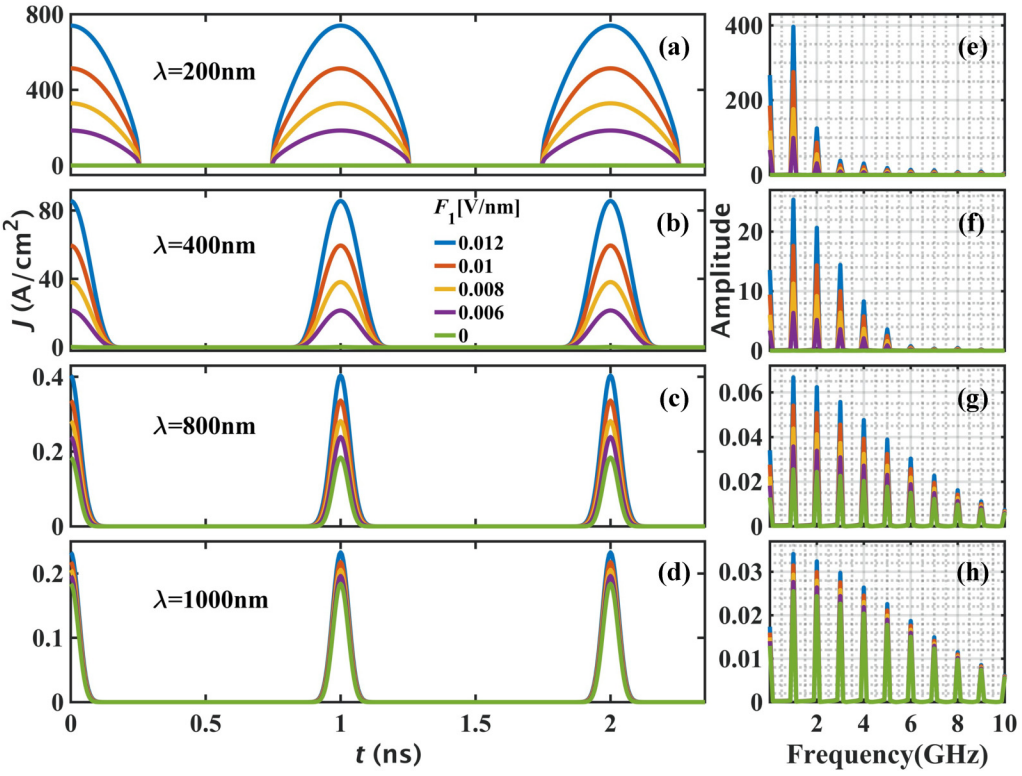

FIG. 6. The effect of laser wavelength on emission current density J. (a)–(d) $\lambda = 200$, 400, 800, and 1000 nm, respectively. (e)–(h) Amplitude spectra of the emission current density at multiples of RF frequency, corresponding to (a)–(d), respectively. RF field amplitude $A = 2$ V/nm.

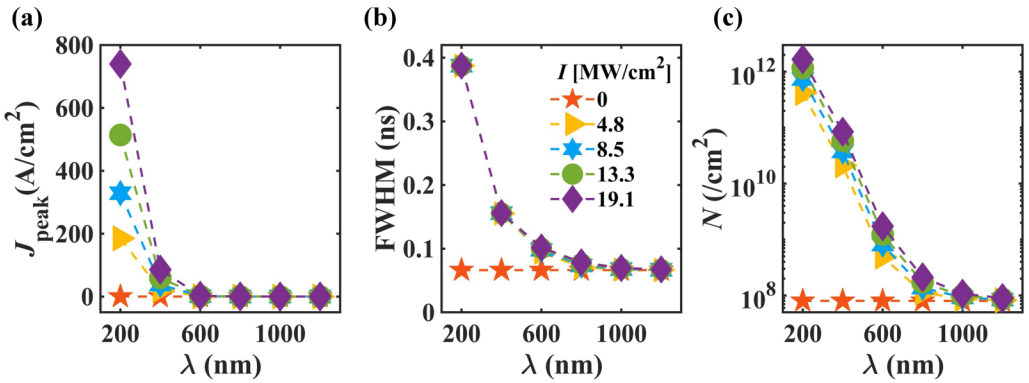

FIG. 7. (a) Peak emission current density, (b) full-width at half maximum (FWHM), and (c) number of emitted electrons in a half RF cycle, as a function of laser wavelength under various laser intensities. RF field amplitude $A = 2$ V/nm. The corresponding laser field strength is $F_1 = 0,\ 0.006,\ 0.008,\ 0.01,\ 0.012$ V/nm for the intensity of $I = 0,\ 4.8,\ 8.5,\ 13.3,\ 19.1$ MW/cm^2.

amplitude spectra of emission current density at multiples of RF frequency (1 GHz) using FFT, corresponding to Figs. 6(a)–6(d), respectively. It is obvious that as laser wavelength increases, there appear more higher-harmonic contents in the density-modulated electron beam.

The effect of laser wavelength on the modulation of emission current (i.e., peak emission current density, FWHM, and the number of emission electrons per RF cycle) is shown in Fig. 7. Figure 7(a) shows the peak emission current density as a function of the laser wavelength range from 200 to 1200 nm with an interval

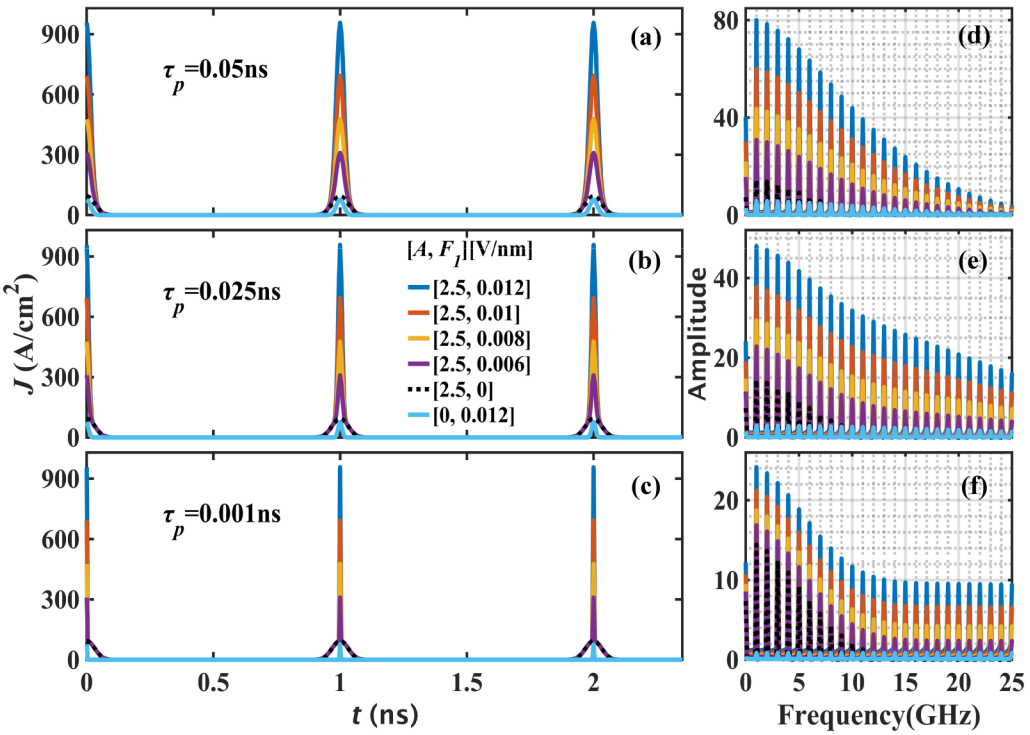

FIG. 8. Emission current density temporal profile under pulsed laser of full-width at half maximum (a) $\tau_p = 0.05$ ns; (b) $\tau_p = 0.025$ ns; (c) $\tau_p = 0.001$ ns. (d)–(f) Amplitude spectra of the emission current density at multiples of RF frequency corresponding to (a)–(c), respectively. The laser wavelength is 200 nm and $A = 2.5$ V/nm. The corresponding laser intensity is $I = 19.1,\ 13.3,\ 8.5, 4.8, 0$ MW/cm^2 for $F_1 = 0.012,\ 0.01,\ 0.008,\ 0.006,\ 0$ V/nm.

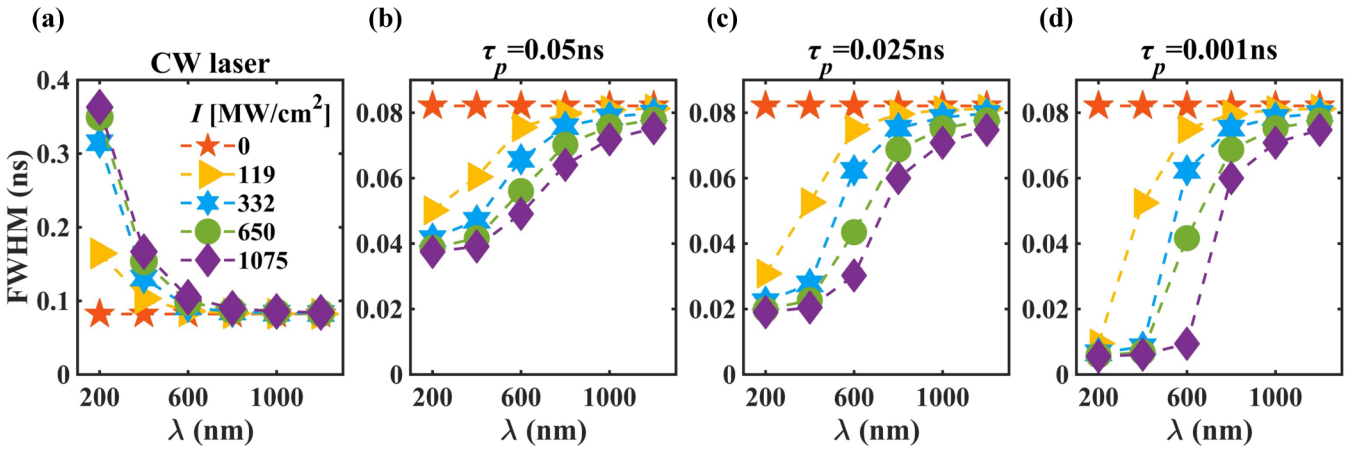

FIG. 9. FWHM of the emission current density as a function of laser wavelength under various laser intensities for (a) continuous-wave laser field; (b) pulsed laser of duration $\tau_p = 0.05$ ns; (c) $\tau_p = 0.025$ ns; and (d) $\tau_p = 0.001$ ns. Here, RF field amplitude $A = 3$ V/nm. The corresponding laser intensity is $I =$ 0, 119, 332, 650, 1075 MW/cm^2 for $F_1 = 0$, 0.03, 0.05, 0.07, 0.09 V/nm.

of 200. It is apparent the peak emission current density decreases quickly when the laser wavelength λ changes from 200 to 600 nm and then levels off for longer wavelengths, where the peak current density is also insensitive to the laser intensity. Figure 7(b) shows the FWHM of the current pulse decreases rapidly with λ changing from 200 to 1200 nm. Also, increasing laser intensities from 4.8 to 19.1 MW/cm^2 has little influence on the FWHM of the current pulse with fixed λ. Figure 7(c) shows the number of emitted electron fluxes per RF cycle, N, in different wavelengths. When the laser intensity is fixed at 19.1 MW/cm^2, the number of emitted electrons is 1.6×10^{12}, 8.4×10^{10}, 1.7×10^{9}, 2.1×10^{8}, 1.1×10^{8}, 9.0×10^{7} with wavelength being 200, 400, 600, 800, 1000, 1200 nm, respectively. It is noticeable that N shows similar trends as peak emission current density. This indicates again that, for CW lasers, the laser intensity has a stronger influence on the emission current amplitude and a smaller influence on the beam width.

B. Electron emission under RF field and pulsed laser field

In this section, we consider electron emission under an RF field and a pulsed laser field [Fig. 2(b)]. For simplicity, we assume the peak of the laser field aligns with the peak of the RF field in all the pulsed laser calculations. Figure 8 shows the emission current density temporal profile and corresponding FFT amplitude spectra, for laser pulses of $\tau_p = 0.05$, 0.025, and 0.001 ns. As the laser pulse length decreases, the emitted electron beam width decreases, while the peak emission current density stays the same for a fixed

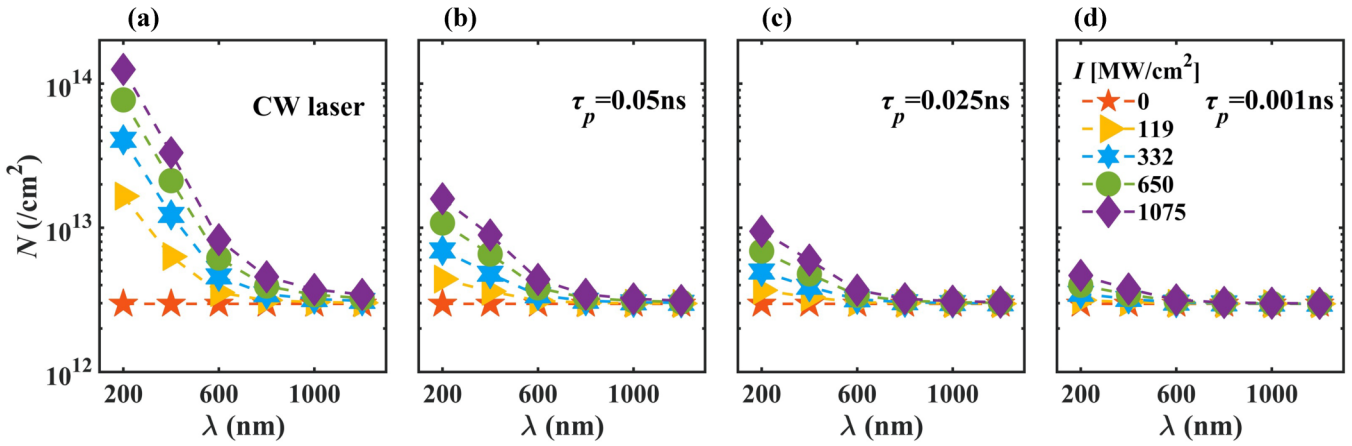

FIG. 10. The number density of emitted electrons per RF cycle as a function of laser intensity under different wavelengths for (a) continuous-wave laser field; (b) pulsed laser of duration $\tau_p = 0.05$ ns; (c) $\tau_p = 0.025$ ns; and (d) $\tau_p = 0.001$ ns. Here, RF field amplitude $A = 3$ V/nm.

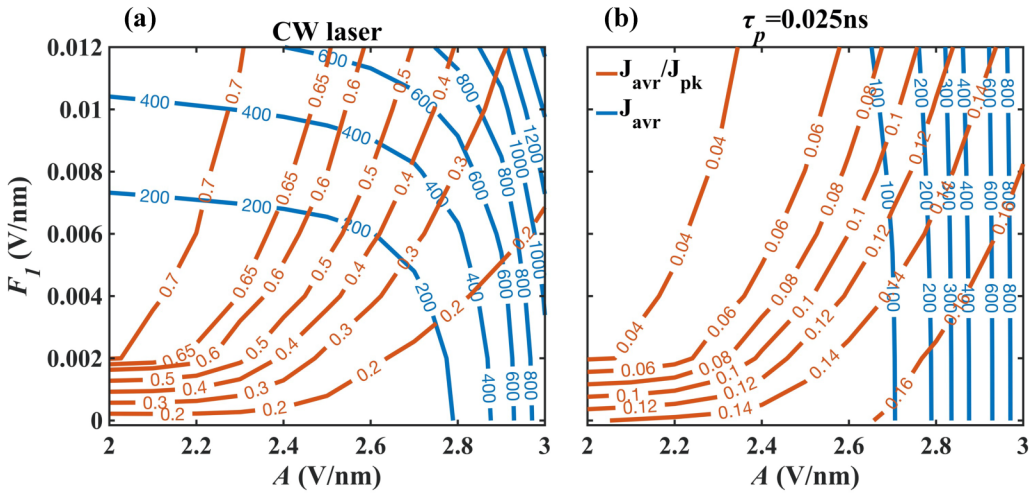

FIG. 11. Average current density J_{avr} (A/cm^2) and the ratio of average over the peak of current density J_{avr}/J_{pk} in various RF amplitude and laser field with 200 nm wavelength for (a) CW laser, and (b) pulsed laser of duration $\tau_p = 0.025$ ns.

laser field. For a given RF field amplitude A and laser pulse duration τ_p, peak emission current density increases, but beam width decreases when F_1 increases. Compared to the RF field only case (black dotted lines), the emission current density induced by combined RF and laser fields is increased by more than 10 times. In comparison with the emission current density under a CW laser field [Figs. 4(a)–4(c)], the width of the electron beam becomes narrower and can be controlled by the laser pulse duration. Figures 8(d)–8(f) show the FFT amplitude spectra at multiples of RF frequency accordingly. For each τ_p, the amplitude of the spectra decreases with frequency. As τ_p decreases, the reduction of higher harmonics becomes slower. Compared with the CW laser field (Figs. 4 and 6), pulsed laser-induced electron emission has higher-harmonic terms.

Figure 9 shows the effects of laser pulse duration on the FWHM of the emitted current density. For comparison, the width of the emission current density for a CW laser with $A = 3$ V/nm is shown in Fig. 9(a), which has a similar trend as in Fig. 7(b). For a pulsed laser, the pulse width of the emission current density increases with laser wavelength for a given laser intensity, while it decreases with the laser intensity for a given laser wavelength. The emitted current pulse width is more sensitive to laser intensity for shorter laser wavelengths.

Figure 10 shows the number density of emitted electrons per RF cycle N under laser fields of various durations. It can be found that N decreases when the wavelength increases or laser intensity decreases. As the pulsed laser duration decreases, N becomes less sensitive to laser intensity and wavelength.

Figure 11 shows contours of constant average current density J_{avr} and the ratio of average over the peak of current density J_{avr}/J_{pk} calculated using our quantum electron emission model in Eq. (2), where Fig. 11(a) is for CW laser, and Fig. 11(b) is for pulsed laser with duration $\tau_p = 0.025$ ns. It shows that both density J_{avr} and J_{avr}/J_{pk} can be adjusted over a wide range of values by controlling RF amplitude, laser field, and laser pulse duration. It shows significantly increased flexibility to achieve density modulation during electron emission over a wide range of parameter space by using optical means, as compared to voltage-controlled field emission (cf. Fig. 14 of Ref. 32). J_{avr}/J_{pk} as small as 0.04 can be achieved using pulsed lasers as shown in Fig. 11(b), which is an order of magnitude smaller than the typical value of $J_{avr}/J_{pk} > 0.3$ from voltage-controlled field emission.[31,32]

IV. SUMMARY

We demonstrate various pulse shapes of pre-bunched electron beams emitted from an RF cold cathode under different combinations of RF field and optical field (continuous-wave or pulsed). The profile of the produced emission current can be modulated by varying RF field (amplitude and frequency) and optical field (laser wavelength, laser intensity, pulse length). The emission current pulse amplitude, beam width (i.e., FWHM of the current pulse), electron numbers per pulse, as well as the harmonic spectrum, are investigated in detail under various combinations of RF and optical fields. The results confirm that photo-assisted field emission under the combination of RF field and optical field is significantly larger than electron emission due to either the RF field or optical field alone. For CW photon sources in the UV to NIR range (i.e., 200–1200 nm), increasing the optical intensity under an RF bias tends to change the shape of the current emission pulse from a Gaussian-like profile toward a sinusoidal-like profile, thus offering great flexibility to control the harmonic contents in electron beam current emission. Pulsed photon sources together with an RF field can produce sharp, high-current electron bunches with pulse duration comparable with or even less than that of the optical pulse. We have also provided a contour map to show a wide range of average current density and density modulation depth (in terms of the ratio of average-to-peak current density), by controlling the RF field and

laser field (either CW or pulsed). The results provide insight into unlocking new opportunities to achieve direct density modulation during electron current emission using optical means, which may be utilized to enhance the operational efficiency of free-electron beam-based electronics, such as TWTs or particle accelerators.

It is worthwhile to note that our results have ignored the effects of space charge,[17,70] which is expected to not only change the surface barrier during emission but also modify the shape of the initially emitted electron bunches during its transport. The former requires consistent calculation by considering the Poisson equation[71,72] during electron emission, whereas the latter needs careful examination of electron dynamics after their emission from the cathode surface.[73–75] Future works are planned to quantify these effects in directly density-modulated electron beams.

Further studies may also include the effects of field enhancement factors for both RF and optical fields for a given emitter and uncertainty quantification of their impact on the pulse shape of the emitted electron bunches. Also, practical implementation of photo-assisted field emission needs to address issues such as laser jitter and alignment,[76,77] as well as geometrical and material effects of the electron emission system.

ACKNOWLEDGMENTS

The work was supported by the Office of Naval Research (ONR) YIP Grant No. N00014-20-1-2681, the Air Force Office of Scientific Research (AFOSR) Grant No. FA9550-20-1-0409, the Air Force Office of Scientific Research (AFOSR) Grant No. FA9550-22-1-0523, and the NSF-DOE Partnership Grant No. DE-SC0022078.

AUTHOR DECLARATIONS

Conflict of Interest

The authors have no conflicts to disclose.

Author Contributions

Lan Jin: Data curation (equal); Formal analysis (equal); Investigation (equal); Methodology (equal); Validation (equal); Visualization (equal); Writing – original draft (equal); Writing – review & editing (equal). **Yang Zhou:** Investigation (equal); Resources (equal); Writing – review & editing (equal). **Peng Zhang:** Conceptualization (lead); Formal analysis (equal); Funding acquisition (equal); Investigation (equal); Methodology (equal); Project administration (equal); Supervision (equal); Validation (equal); Writing – review & editing (equal).

DATA AVAILABILITY

The data that support the findings of this study are available from the corresponding author upon reasonable request.

REFERENCES

[1]K. L. Jensen, *Introduction to the Physics of Electron Emission*, 1st ed. (Wiley, Hoboken, NJ, 2017).
[2]A. V. Burdakov, A. V. Arzhannikov, V. S. Burmasov, I. A. Ivanov, M. V. Ivantsivsky, I. V. Kandaurov, S. A. Kuznetsov, V. V. Kurkuchekov, K. I. Mekler, S. V. Polosatkin, S. S. Popov, V. V. Postupaev, A. F. Rovenskikh, V. F. Sklyarov, M. K. A. Thumm, Y. A. Trunev, and L. N. Vyacheslavov, "Microwave generation during 100 keV electron beam relaxation in GOL-3," Fusion Sci. Technol. **63**(1T), 286–288 (2013).
[3]R. J. England, R. J. Noble, K. Bane, D. H. Dowell, C.-K. Ng, J. E. Spencer, S. Tantawi, Z. Wu, R. L. Byer, E. Peralta, K. Soong, C.-M. Chang, B. Montazeri, S. J. Wolf, B. Cowan, J. Dawson, W. Gai, P. Hommelhoff, Y.-C. Huang, C. Jing, C. McGuinness, R. B. Palmer, B. Naranjo, J. Rosenzweig, G. Travish, A. Mizrahi, L. Schachter, C. Sears, G. R. Werner, and R. B. Yoder, "Dielectric laser accelerators," Rev. Mod. Phys. **86**(4), 1337–1389 (2014).
[4]T. Popmintchev, M.-C. Chen, D. Popmintchev, P. Arpin, S. Brown, S. Ališauskas, G. Andriukaitis, T. Balčiunas, O. D. Mücke, A. Pugzlys, A. Baltuška, B. Shim, S. E. Schrauth, A. Gaeta, C. Hernández-García, L. Plaja, A. Becker, A. Jaron-Becker, M. M. Murnane, and H. C. Kapteyn, "Bright coherent ultrahigh harmonics in the keV x-ray regime from mid-infrared femtosecond lasers," Science **336**(6086), 1287–1291 (2012).
[5]M. Tu, B. Xia, D. E. Kravchenko, M. L. Tietze, A. J. Cruz, I. Stassen, T. Hauffman, J. Teyssandier, S. De Feyter, Z. Wang, R. A. Fischer, B. Marmiroli, H. Amenitsch, A. Torvisco, M. J. Velásquez-Hernández, P. Falcaro, and R. Ameloot, "Direct x-ray and electron-beam lithography of halogenated zeolitic imidazolate frameworks," Nat. Mater. **20**(1), 93–99 (2021).
[6]G. N. Fursey, "Field emission in vacuum micro-electronics," Appl. Surf. Sci. **215**(1–4), 113–134 (2003).
[7]C. M. Armstrong, E. C. Snively, M. Shumail, C. Nantista, Z. Li, S. Tantawi, B. W. Loo, R. J. Temkin, R. G. Griffin, J. Feng, R. Dionisio, F. Mentgen, N. Ayllon, M. A. Henderson, and T. P. Goodman, "Frontiers in the application of RF vacuum electronics," IEEE Trans. Electron Devices **70**, 2643–2655 (2023).
[8]P. Wong, P. Zhang, and J. Luginsland, "Recent theory of traveling-wave tubes: A tutorial-review," Plasma Res. Express **2**(2), 023001 (2020).
[9]D. Shiffler, T. K. Statum, T. W. Hussey, O. Zhou, and P. Mardahl, *Wave Power Electron* (IEEE, Piscataway, NJ, 2005), p. 691.
[10]Y. Zhu and H. Dürr, "The future of electron microscopy," Phys. Today **68**(4), 32–38 (2015).
[11]A. Grillo, J. Barrat, Z. Galazka, M. Passacantando, F. Giubileo, L. Iemmo, G. Luongo, F. Urban, C. Dubourdieu, and A. Di Bartolomeo, "High field-emission current density from β-Ga_2O_3 nanopillars," Appl. Phys. Lett. **114**(19), 193101 (2019).
[12]S. Sun, X. Sun, D. Bartles, E. Wozniak, J. Williams, P. Zhang, and C.-Y. Ruan, "Direct imaging of plasma waves using ultrafast electron microscopy," Struct. Dyn. **7**(6), 064301 (2020).
[13]S. Banerjee and P. Zhang, "Scaling of time-dependent tunneling current in terahertz scanning tunneling microscopes," Phys. Rev. Appl. **18**(2), 024011 (2022).
[14]H. R. Kaufman, *The Neutralization of Ion-Rocket Beams* (National Aeronautics and Space Administration, 1961).
[15]P. Zhang and Y. Y. Lau, "Ultrafast and nanoscale diodes," J. Plasma Phys. **82**(5), 595820505 (2016).
[16]J. Lin, P. Y. Wong, P. Yang, Y. Y. Lau, W. Tang, and P. Zhang, "Electric field distribution and current emission in a miniaturized geometrical diode," J. Appl. Phys. **121**(24), 244301 (2017).
[17]P. Zhang, Y. S. Ang, A. L. Garner, Á. Valfells, J. W. Luginsland, and L. K. Ang, "Space–charge limited current in nanodiodes: Ballistic, collisional, and dynamical effects," J. Appl. Phys. **129**(10), 100902 (2021).
[18]S. Banerjee and P. Zhang, "Review of recent studies on nanoscale electrical junctions and contacts: Quantum tunneling, current crowding, and interface engineering," J. Vac. Sci. Technol. A **40**(3), 030802 (2022).
[19]J. Benford, J. A. Swegle, and E. Schamiloglu, *High Power Microwaves*, 3rd ed. (CRC Press, 2015).
[20]J. H. Booske, "Plasma physics and related challenges of millimeter-wave-to-terahertz and high power microwave generation," Phys. Plasmas **15**(5), 055502 (2008).
[21]A. S. Gilmour, Jr., *Principles of Traveling Wave Tubes* (Artech Print on Demand, Boston, 1994).

[22]P. Zhang, L. K. Ang, and A. Gover, "Enhancement of coherent Smith–Purcell radiation at terahertz frequency by optimized grating, prebunched beams, and open cavity," Phys. Rev. Spec. Top. Accel. Beams **18**(2), 020702 (2015).
[23]M. A. Faisal and P. Zhang, "Grating optimization for Smith–Purcell radiation: Direct correlation between spatial growth rate and starting current," IEEE Trans. Electron Devices **70**, 2860–2863 (2023).
[24]D. H. Simon, B. W. Hoff, J. A. Schrock, S. Beeson, W. Tang, P. D. Lepell, T. Montoya, D. M. French, and S. L. Heidger, "Experiments on a disk-on-rod traveling wave tube amplifier driven by a nonlinear transmission line modulated electron beam," IEEE Trans. Plasma Sci. **50**(2), 236–240 (2022).
[25]V. L. Granatstein, R. K. Parker, and C. M. Armstrong, "Vacuum electronics at the dawn of the twenty-first century," Proc. IEEE **87**(5), 702–716 (1999).
[26]M. A. Kodis, K. L. Jensen, E. G. Zaidman, B. Goplen, and D. N. Smithe, "Operation and optimization of gated field emission arrays in inductive output amplifiers," IEEE Trans. Plasma Sci. **24**(3), 970–981 (1996).
[27]G. A. Espersen, "Principles of electron tubes including grid-controlled tubes, microwave tubes and gas tubes," Proc. IEEE **53**(8), 1166 (1965).
[28]D. H. Simon, P. Wong, D. Chernin, Y. Y. Lau, B. Hoff, P. Zhang, C. F. Dong, and R. M. Gilgenbach, "On the evaluation of pierce parameters C and Q in a traveling wave tube," Phys. Plasmas **24**(3), 033114 (2017).
[29]A. V. Haeff and L. S. Nergaard, "A wide-band inductive-output amplifier," Proc. IRE **28**(3), 126–130 (1940).
[30]A. J. Lichtenberg, "Prebunched beam traveling-wave tube studies," IRE Trans. Electron Devices **9**(4), 345–351 (1962).
[31]D. R. Whaley, B. M. Gannon, C. R. Smith, C. M. Armstrong, and C. A. Spindt, "Application of field emitter arrays to microwave power amplifiers," IEEE Trans. Plasma Sci. **28**(3), 727–747 (2000).
[32]D. R. Whaley, B. M. Gannon, V. O. Heinen, K. E. Kreischer, C. E. Holland, and C. A. Spindt, "Experimental demonstration of an emission-gated traveling-wave tube amplifier," IEEE Trans. Plasma Sci. **30**(3), 998–1008 (2002).
[33]K. L. Jensen, Y. Y. Lau, and D. S. McGregor, "Analysis of a photon assisted field emission device," Appl. Phys. Lett. **77**(4), 585–587 (2000).
[34]C. M. Armstrong, "The quest for the ultimate vacuum tube," IEEE Spectr. **52**(12), 28–51 (2015).
[35]K. L. Jensen, Y. Y. Lau, and D. McGregor, "Photon assisted field emission from a silicon emitter," Solid-State Electron. **45**(6), 831–840 (2001).
[36]P. Hommelhoff, Y. Sortais, A. Aghajani-Talesh, and M. A. Kasevich, "Field emission tip as a nanometer source of free electron femtosecond pulses," Phys. Rev. Lett. **96**(7), 077401 (2006).
[37]R. Bormann, M. Gulde, A. Weismann, S. V. Yalunin, and C. Ropers, "Tip-enhanced strong-field photoemission," Phys. Rev. Lett. **105**(14), 147601 (2010).
[38]P. Tallerico, R. Sheffield, W. Cornelius, E. Gray, M. Wilson, D. Nguyen, K. Meier, and R. Stockley, "An RF-driven lasertron," in Proceedings of the 1988 Linear Accelerator Conference, Williamsburg, VA, 3-7 October 1988.
[39]E. L. Garwin, W. B. Herrmannsfeldt, C. Sinclair, J. N. Weaver, J. J. Welch, and P. B. Wilson, "An experimental program to build a multimegawatt lasertron for super linear colliders," IEEE Trans. Nucl. Sci. **32**(5), 2906–2908 (1985).
[40]W. W. Tang, D. A. Shiffler, J. R. Harris, K. L. Jensen, K. Golby, M. LaCour, and T. Knowles, "Field emission characteristics of a small number of carbon fiber emitters," AIP Adv. **6**(9), 095007 (2016).
[41]W. Tang, D. Shiffler, K. Golby, M. LaCour, and T. Knowles, "Experimental study of electric field screening by the proximity of two carbon fiber cathodes," J. Vac. Sci. Technol. B **30**(6), 061803 (2012).
[42]T. A. Spencer, K. J. Hendricks, M. D. Haworth, M. D. Mitchell, M. D. Sena, M. J. LaCour, and D. A. Shiffler, "Comparison of carbon fiber and cesium iodide-coated carbon fiber cathodes," IEEE Trans. Plasma Sci. **28**(3), 517–522 (2000).
[43]D. Shiffler, S. Fairchild, W. Tang, B. Maruyama, K. Golby, M. LaCour, M. Pasquali, and N. Lockwood, "Demonstration of an acid-spun single-walled nanotube fiber cathode," IEEE Trans. Plasma Sci. **40**(7), 1871–1877 (2012).
[44]S. B. Fairchild, J. Boeckl, T. C. Back, J. B. Ferguson, H. Koerner, P. T. Murray, B. Maruyama, M. A. Lange, M. M. Cahay, N. Behabtu, C. C. Young, M. Pasquali, N. P. Lockwood, K. L. Averett, G. Gruen, and D. E. Tsentalovich, "Morphology dependent field emission of acid-spun carbon nanotube fibers," Nanotechnology **26**(10), 105706 (2015).
[45]P. Zhang, S. B. Fairchild, T. C. Back, and Y. Luo, "Field emission from carbon nanotube fibers in varying anode-cathode gap with the consideration of contact resistance," AIP Adv. **7**(12), 125203 (2017).
[46]P. Zhang, J. Park, S. Fairchild, N. Lockwood, Y. Lau, J. Ferguson, and T. Back, "Temperature comparison of looped and vertical carbon nanotube fibers during field emission," Appl. Sci. **8**(7), 1175 (2018).
[47]S. B. Fairchild, P. Zhang, J. Park, T. C. Back, D. Marincel, Z. Huang, and M. Pasquali, "Carbon nanotube fiber field emission array cathodes," IEEE Trans. Plasma Sci. **47**(5), 2032–2038 (2019).
[48]S. B. Fairchild, C. E. Amanatides, T. A. De Assis, P. T. Murray, D. Tsentalovich, J. L. Ellis, S. Portillo, S. R. Kanel, J. S. Bulmer, J. Park, G. Dion, and J. J. Boeckl, "Field emission cathodes made from knitted carbon nanotube fiber fabrics," J. Appl. Phys. **133**(9), 094302 (2023).
[49]S. Ji, L. Piazza, G. Cao, S. T. Park, B. W. Reed, D. J. Masiel, and J. Weissenrieder, "Influence of cathode geometry on electron dynamics in an ultrafast electron microscope," Struct. Dyn. **4**(5), 054303 (2017).
[50]P. Zhang and Y. Y. Lau, "Ultrafast strong-field photoelectron emission from biased metal surfaces: Exact solution to time-dependent Schrödinger equation," Sci. Rep. **6**(1), 19894 (2016).
[51]Y. Luo and P. Zhang, "Analysis of two-color laser-induced electron emission from a biased metal surface using an exact quantum mechanical solution," Phys. Rev. Appl. **12**(4), 044056 (2019).
[52]Y. Luo, Y. Zhou, and P. Zhang, "Few-cycle optical-field-induced photoemission from biased surfaces: An exact quantum theory," Phys. Rev. B **103**(8), 085410 (2021).
[53]Y. Zhou and P. Zhang, "Unraveling quantum pathways interference in two-color coherent control of photoemission with bias voltages," Phys. Rev. B **106**(8), 085402 (2022).
[54]J. W. Lewellen and J. Noonan, "Field-emission cathode gating for rf electron guns," Phys. Rev. Spec. Top. Accel. Beams **8**(3), 033502 (2005).
[55]G. A. Mesyats, "Ecton mechanism of the cathode spot phenomena in a vacuum arc," IEEE Trans. Plasma Sci. **41**(4), 676–694 (2013).
[56]Y. Zhou and P. Zhang, "A quantum model for photoemission from metal surfaces and its comparison with the three-step model and Fowler–DuBridge model," J. Appl. Phys. **127**(16), 164903 (2020).
[57]Y. Zhou and P. Zhang, "Quantum efficiency of photoemission from biased metal surfaces with laser wavelengths from UV to NIR," J. Appl. Phys. **130**(6), 064902 (2021).
[58]Y. Zhou and P. Zhang, "Theory of laser-induced photoemission from a metal surface with nanoscale dielectric coating," J. Appl. Phys. **131**(6), 064903 (2022).
[59]X. Xiong, Y. Zhou, Y. Luo, X. Li, M. Bosman, L. K. Ang, P. Zhang, and L. Wu, "Plasmon-enhanced resonant photoemission using atomically thick dielectric coatings," ACS Nano **14**(7), 8806–8815 (2020).
[60]Y. Luo, J. Luginsland, and P. Zhang, "Interference modulation of photoemission from biased metal cathodes driven by two lasers of the same frequency," AIP Adv. **10**(7), 075301 (2020).
[61]Y. Luo and P. Zhang, "Ultrafast strong-field photoelectron emission due to two-color laser fields," Phys. Rev. B **98**(16), 165442 (2018).
[62]Y. Zhou and P. Zhang, "Theory of field emission from dielectric coated surfaces," Phys. Rev. Res. **2**(4), 043439 (2020).
[63]Y. Luo and P. Zhang, "Ultrafast optical-field-induced photoelectron emission in a vacuum nanoscale gap: An exact analytical formulation," Appl. Phys. Lett. **119**(19), 194101 (2021).
[64]Y. Luo and P. Zhang, "Optical-field-induced electron emission in a dc-biased nanogap," Phys. Rev. Appl. **17**(4), 044008 (2022).
[65]R. G. Forbes, "Physics of generalized Fowler–Nordheim-type equations," J. Vac. Sci. Technol. B **26**(2), 788 (2008).

[66]S. Keramati, A. Passian, V. Khullar, J. Beck, C. Uiterwaal, and H. Batelaan, "Surface plasmon enhanced fast electron emission from metallised fibre optic nanotips," New J. Phys. **22**(8), 083069 (2020).
[67]Y. Zhou, R. Ahsan, H. U. Chae, R. Kapadia, and P. Zhang, "Theoretical analysis of resonant tunneling enhanced field emission," Phys. Rev. Appl. **20**(1), 014043 (2023).
[68]J. H. Bechtel, "Heating of solid targets with laser pulses," J. Appl. Phys. **46**(4), 1585–1593 (1975).
[69]R. H. Fowler and L. Nordheim, "Electron emission in intense electric fields," Proc. R. Soc. Lond. Ser. Contain. Pap. Math. Phys. Character **119**(781), 173–181 (1928).
[70]P. Zhang, Á. Valfells, L. K. Ang, J. W. Luginsland, and Y. Y. Lau, "100 years of the physics of diodes," Appl. Phys. Rev. **4**(1), 011304 (2017).
[71]P. Zhang, "Scaling for quantum tunneling current in nano- and subnano-scale plasmonic junctions," Sci. Rep. **5**(1), 9826 (2015).
[72]S. Banerjee and P. Zhang, "A generalized self-consistent model for quantum tunneling current in dissimilar metal-insulator-metal junction," AIP Adv. **9**(8), 085302 (2019).
[73]Y. L. Liu, P. Zhang, S. H. Chen, and L. K. Ang, "Maximal charge injection of consecutive electron pulses with uniform temporal pulse separation," Phys. Plasmas **22**(8), 084504 (2015).
[74]Y. L. Liu, P. Zhang, S. H. Chen, and L. K. Ang, "Maximal charge injection of a uniform separated electron pulse train in a drift space," Phys. Rev. Spec. Top. Accel. Beams **18**(12), 123402 (2015).
[75]C. Kaur, K. Rambabu, and R. Fedosejevs, "High-current space-charge-limited pulses using ultrashort laser pulses," Phys. Rev. E **106**(5), 055203 (2022).
[76]M. A. McEver, "Adaptive feedback control of optical jitter using Q-parameterization," Opt. Eng. **43**(4), 904 (2004).
[77]D. Kim, J. J. Kim, D. Frist, M. Nagashima, and B. Agrawal, "High energy laser testbed for accurate beam pointing control," Proc. SPIE **7587**, 75870G (2010).